Tellus (1999), 51B, 616–628
Printed in UK. All rights reserved

TELLUS
ISSN 0280–6509

The rôle of capillary waves in oceanic air/water gas exchange

By J. R. SAYLOR,* *Naval Research Laboratory, Washington, DC 20375, USA*

(Manuscript received 5 December 1997; in final form 15 September 1998)

ABSTRACT

Recent experiments have demonstrated that millimeter-scale capillary waves can enhance the transport of CO_2 by almost 2 orders of magnitude for moderate wave slopes. These results are used to create a model for the relative contribution of capillary waves to the gas exchange coefficient. The model input is wind speed u, and the output is K_f the fractional contribution of a specific range of capillary waves to the total gas exchange coefficient. Wind speed data, obtained via satellite, are used as the model input to obtain globally averaged values for K_f. In spite of the enhancing effect which capillary waves provide in the laboratory, the maximum value of K_f predicted by the model is less than 10%, and global averages are less than 4%. The small values of K_f are primarily due to the small wave energies predicted by existing wave height spectra in the high wave number regime. The uncertainty in existing wave height spectra, and the importance of experimental validation of the high wave number regime is discussed. Some interesting aspects of capillary wave gas exchange are also expanded upon. Among these are the demonstration of a linear relationship between the capillary wave gas exchange coefficient and wavelength, and a peak in the contribution of capillary waves to gas exchange at a wavelength around $\lambda = 3.6$ mm.

1. Introduction

The oceans possess an enormous capacity to absorb heat and dissolved gases. Accordingly, an accurate understanding of the processes which govern the transport of heat and mass across the air/sea interface is necessary for the prediction of weather and the long term behavior of the atmosphere. Capillary waves are expected to have an important contribution to the transport of heat and mass. However the mechanisms responsible for this contribution are poorly understood. Measurements of gas exchange coefficients conducted in wind/wave tunnels or on the open sea, have succeeded in parameterizing the gas exchange coefficient to wind speed or to the mean square wave slope (Ocampo-Torres et al., 1994; Jähne et al., 1979; Jähne et al., 1985; Jähne et al., 1987; Broecker, et al., 1978). In these wind/wave tunnel studies, however, many phenomena, such as turbulence, bubble generation, wave breaking, etc. coexist, preventing one from ascertaining the contribution of capillary waves to the overall transport process. A true understanding of how capillary waves contribute to transport requires that these waves be isolated from all other transport-enhancing effects.

Saylor and Handler (1997) isolated capillary waves and investigated their ability to enhance the transfer of CO_2 across an air/water interface. A uniform, monochromatic field of capillary waves was used to study these waves independent of any other phenomena which might enhance transport. These capillary waves were Faraday waves (Faraday, 1831) generated by vibrating a small tank in the vertical direction. The theory describing these waves has been investigated by several

E-mail: j.r.saylor@nrl.navy.mil

authors (Benjamin and Ursell, 1954; Miles, 1993; Henderson and Miles, 1990; Henderson and Miles, 1991; Milner, 1991; Vanden-Broeck, 1984; Christiansen et al., 1995) and a review can be found in Miles and Henderson (1990).

At very low vibration amplitudes, Faraday waves are pure standing waves, where the nodes and anti-nodes of the wave pattern are fixed in space. At larger excitation amplitudes, the wave pattern becomes unstable and exhibits a random drifting motion, which has been explained as a random Stokes drift (Mesquita et al., 1992). The experiments of Saylor and Handler (1997) were all conducted at amplitudes for which the wave field exhibited this drifting behavior. Because it is suspected that the trough of the wave is the region where significant enhancement of gas exchange occurs (Szeri, 1997), this drift is important, since without it only a fraction of the water surface would be exposed to this trough area. The drift of the wave field ensures that, as is the case for a progressive wave, all portions of the water surface are exposed to all phases of the wave cycle.

Transport is quantified by the gas exchange coefficient K which is defined in eq. (1)

$$C_w = \left(C_{w,0} - \frac{C_a}{H}\right) e^{(-K/h)t} + \frac{C_a}{H}, \qquad (1)$$

where C_w is the concentration of CO_2 in the water, C_a is the concentration of CO_2 in the air, h is the height of the water, H is the Henry's law constant which accounts for the degree of solubility of CO_2 in the water, t is time, and $C_{w,0}$ is the concentration at $t = 0$. During the experiments of Saylor and Handler (1997), C_w was recorded as a function of time and a plot of C_w versus t yielded a straight line of slope $-K/h$, when plotted on semi-logarithmic coordinates. Values for K were obtained by performing a least squares fit to these semi-logarithmic time traces of CO_2 concentration. By vibrating the tank at different amplitudes, different wave slopes S were obtained for a given wavelength λ. Experiments were run at four different values of λ and over a range of wave slopes. The wave slope was measured during the course of these experiments, and K was correlated to $\overline{S^2}$, the mean square wave slope. Additional details concerning the experimental procedure and apparatus can be found in Saylor and Handler (1997).

A summary of the results obtained from the aforementioned experiments is presented in Fig. 1, where K is plotted against $\overline{S^2}$ for the four different wavelengths investigated, $\lambda = 2.26$, 2.87, 3.19 and 3.62 mm. The solid lines faired through each data set are linear least-squares regressions of the form:

$$K = C\overline{S^2}, \qquad (2)$$

where the y-intercept for the fit has been constrained to be zero. The values for C used in eq. (2) are listed in Table 1. In Saylor and Handler (1997), the linear curve fit was performed without the zero intercept constraint, and a small, but non-zero value of K at $\overline{S^2} = 0$ was obtained. This non-zero value is due to the small amount of background natural convection and diffusion which exists in the absence of wave motion. In the current work, we are investigating the contribution of capillary waves to overall transport, and hence by definition K must be zero when $\overline{S^2} = 0$.

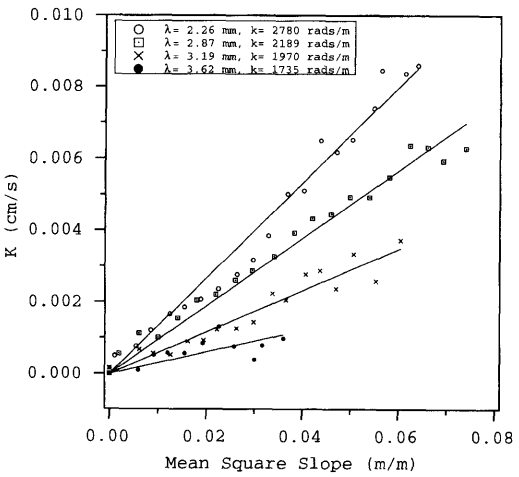

Fig. 1. Plot of K versus mean square wave slope $\overline{S^2}$, for all four excitation frequencies. A linear curve fit is included for each data set.

Table 1. *Values for the constant C used in eq. (2) corresponding to each value of the wavelength, λ*

λ (mm)	k (rads/m)	C
2.26	2780	0.13302
2.87	2189	0.09430
3.19	1970	0.05783
3.62	1735	0.03013

In any event, as Fig. 1 illustrates, even with this artificial constraint the linear fit is quite good.

The data presented in Fig. 1 show that K increases with both $\overline{S^2}$ and k. More importantly, the values of K obtained are relatively large, approaching 0.01 cm/s. To put this number in perspective, a value of $K = 0.01$ cm/s, in a typical wind/wave tunnel facility, is not usually attained until the wind speed exceeds 10 m/s (e.g. Fig. 6). These results clearly demonstrate that capillary waves can dramatically increase the transport of gas across an air/water interface. What is less obvious is the degree to which such capillary waves actually contribute to gas exchange on the ocean. While the values of $\overline{S^2}$ investigated by Saylor and Handler (1997) (order of 10^{-2} m/m) are typical of wind/wave tunnel facilities (Jähne et al., 1987), and presumably of the ocean, the tank was completely covered by capillary waves in Saylor and Handler (1997), while coverage of the ocean by such waves is expected to be much smaller. Stated another way, the energy possessed by capillary waves in the polychromatic wave field of a typical ocean surface may be so small that their contributions to gas exchange may be minimal, Fig. 1 notwithstanding.

The goal of this paper, then, is to estimate the degree to which capillary waves actually do contribute to the overall oceanic gas exchange coefficient. This is achieved by utilizing existing wave height spectra to determine the energy which exists in the band of wave numbers for which data is presented in Fig. 1. This energy is then used to "weight" the values of K presented in Fig. 1. These weighted values are then scaled to the total gas exchange coefficient K_{tot}, to give K_f, an estimate of the capillary wave contribution to the oceanic transport coefficient. It should be noted that the work presented herein concerns the contribution of capillary waves to K and not to the actual exchange of gas. Prediction of the latter requires knowledge of the differences in CO_2 concentration which exists at the air/sea interface, for which global data is not currently available.

The capillary waves investigated by Saylor and Handler (1997) were Faraday waves which differ from those which exist on the ocean in that they are not progressive waves and are generated by a different driving force. It would be desirable to construct a model for K_f using data obtained from progressive capillary waves. However, obtaining gas exchange data for pure, monochromatic, progressive capillary waves is not possible for the following reasons. Generation of capillary waves via wind shear is inevitably accompanied by turbulence and a polychromatic wave field, preventing the isolation of these waves. The alternative method of generating capillary waves via a paddle or mechanical dipper is no better, since millimeter-scale capillary waves decay too rapidly to permit the creation of a uniform wave field of any significant extent. Therefore, Faraday waves are the best platform for isolating and understanding the transport properties of capillary waves. This point is further addressed in Section 4.

The organization of this paper is as follows. In Section 2 a model of the fractional contribution of capillary waves to gas exchange is developed, which gives K_f as a function of wind speed. Global wind speed data obtained from satellite are used as an input to the K_f model in Section 3 to obtain global month-by-month estimates of K_f. The results are discussed in Section 4 and summarized in Section 5.

2. Method

In this section, a model for K_f is presented, where K_f is the relative contribution of capillary waves to the gas exchange coefficient at a given wind speed. Hence, K_f is defined as

$$K_f = \frac{K_c}{K_{tot}}, \tag{3}$$

where K_{tot} is the total gas exchange coefficient at a given wind speed, and K_c is the portion of K_{tot} attributable to the specific band of capillary waves under consideration. Up to this point we have implicitly referred to capillary waves in the general sense; that is all waves for which $\lambda < 1.7$ cm. However, for the majority of this work, we will consider only the range of wavelengths investigated by Saylor and Handler (1997), since these are the only capillary waves for which monochromatic K versus S data are available. Therefore, K_c is the portion of K_{tot} which can be attributed to $2.26 \text{ mm} \leqslant \lambda \leqslant 3.62$ mm (in a later section, K_c due to the entire range of capillary waves will also be presented). In terms of wave numbers k,

$$k = \frac{2\pi}{\lambda}, \tag{4}$$

K_c represents transport due to the wave number $k_1 \leqslant k \leqslant k_2$, where

$$k_1 = 1735 \text{ rads/m}, \tag{5}$$

$$k_2 = 2780 \text{ rads/m}. \tag{6}$$

In the following two subsections, models for K_c and K_{tot} are developed and then substituted into eq. (3) to construct the model for K_f. In Subsection 2.1, a model for K_c is constructed using wave number spectra and the data presented in Fig. 1. In Subsection 2.2, K_{tot} is obtained from models and data relating the total gas exchange coefficient to wind speed.

2.1. K_c model

The data presented in Fig. 1 show that, for a given capillary wave number (wavelength), the gas exchange coefficient increases as the mean square slope of that wave increases. Assuming that capillary waves behave similarly on the ocean, a measurement of $\overline{S^2}$ for a specific wave number, or range of wave numbers on the ocean, can be used in conjunction with the data of Fig. 1 to obtain K_c. This procedure is developed below, wherein $\overline{S^2}$ for the range of capillary waves under consideration is obtained using existing models of ocean wave height spectra.

The mean square slope, $\overline{S^2}$ is related to the wave height spectrum, Ψ by the following relationship,

$$\overline{S^2} = \int_{k_a}^{k_b} \int_{-\pi}^{\pi} \Psi(k, \theta) k^3 \, \mathrm{d}k \, d\theta, \tag{7}$$

where k_a and k_b define the range of wave numbers between which $\overline{S^2}$ is to be evaluated. Note that in addition to k and θ, Ψ is implicitly dependent on wind speed, u.

Many wave height spectral models exist in the literature. The initial work of Phillips provided a theoretical basis for the description of the spectrum for gravity waves (Phillips, 1958), as well as capillary waves (Phillips, 1966). Many modifications and alternative spectra were subsequently developed, for example the work of Kitaigorodskii (1983), Pierson and Moskowitz (1964), Banner (1990), Allen and Joseph (1990), Wu (1972) and many others. A review can be found in Donelan and Pierson (1987).

The high wave number portion of the spectrum remains poorly understood due to the multiplicity of mechanisms by which capillary waves are created (direct wind interaction, parasitic generation, subsurface turbulence, wave breaking, etc.). Moreover, existing methods of wave height measurement render resolution of the spectra difficult for wave numbers much larger than 1000 rads/m, making experimental confirmation problematic. In the current work, the spectra of Apel (1994) and Elfouhaily et al. (1997) were used in the construction of the K_c model. While these spectra do not resolve all of the uncertainties in the high wave number portion of the spectrum, their combination of theory and experiment provide what is probably the best model of this portion of the spectrum which currently exists.

Both the Apel (1994) spectrum and the Elfouhaily et al. (1997) spectrum (referred to as the A-spectrum and the E-spectrum hereinafter) incorporate ideas and data due to Bjerkaas and Riedel (1979), Donelan and Pierson (1987), Banner (1990), Jähne and Riemer (1990) and Klinke and Jähne (1992). Many portions of the spectra are derived from laboratory data. Each spectrum is derived by compiling several formulas, each dealing with a different aspect of the spectrum, or a different region in wave number space. A plot of the directionally-averaged spectrum, ϕ, where

$$\phi(k) = \int_{-\pi}^{\pi} \Psi(k, \theta) \, \mathrm{d}\theta, \tag{8}$$

is presented in Fig. 2a for the A-spectrum and in Fig. 3a for the E-spectrum. The (b) portion of each of these figures presents the same spectra, focusing on the wave number region, $k_1 \leqslant k \leqslant k_2$. Both spectra assume an exponential decay in the high wave number region of the spectrum. For the A-spectrum, the form of this decay is

$$\exp(-k^2/k_{dis}^2), \tag{9}$$

where k_{dis} is the wave number at which the exponential decay is assumed to dominate, and is arbitrarily set to 6283 rads/m ($\lambda = 1$ mm). The E-spectrum has an exponential decay of the following form,

$$\exp\left\{-\frac{1}{4}\left[\frac{k}{k_m} - 1\right]^2\right\}, \tag{10}$$

where k_m is the wave number for the minimum phase speed.

Once a wind speed u is chosen, $\overline{S^2}$ is obtained using either the A-spectrum or the E-spectrum,

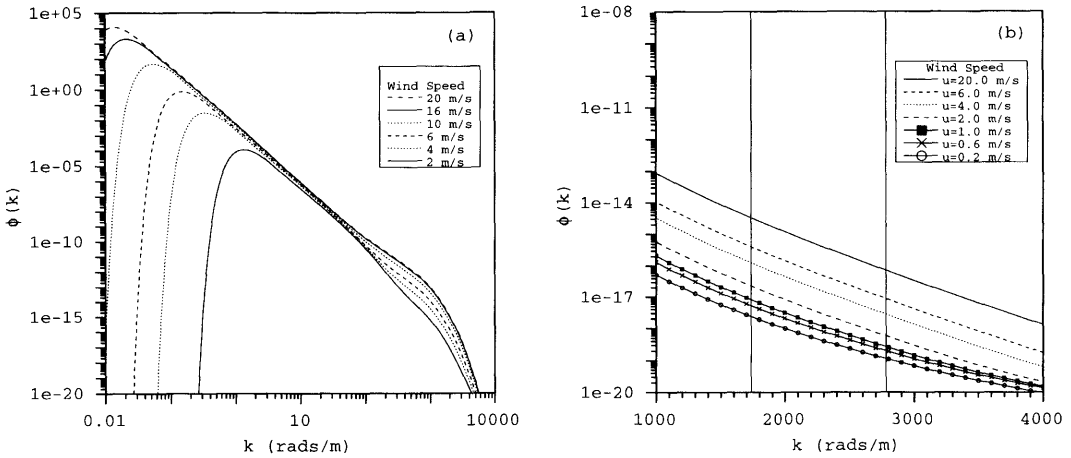

Fig. 2. Plot of wave height spectrum due to Apel (1994). (a) Full spectrum, (b) close up of spectrum for wave numbers $k_1 < k < k_2$. Vertical lines indicate locations of k_1 and k_2.

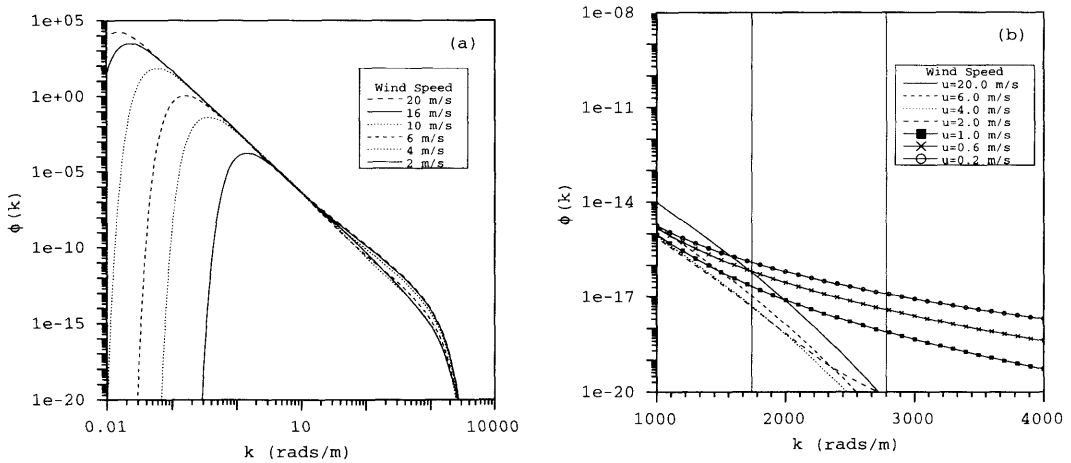

Fig. 3. Plot of wave height spectrum due to Elfouhaily et al. (1997). (a) Full spectrum, (b) close up of spectrum for wave numbers $k_1 < k < k_2$. Vertical lines indicate locations of k_1 and k_2.

for a specific range of wave numbers. Using this value for $\overline{S^2}$, the capillary wave data presented in Fig. 1 is used to obtain K_c for that range of wave numbers. The data, as presented in Fig. 1, is in a somewhat inconvenient form, however. In the subsequent development, values of K will be computed based on wave number and therefore it is more convenient to view K as some function of k. In Fig. 4, the curve fits presented in Fig. 1 are used to obtain four K versus $1/k$ data points at several different values of $\overline{S^2}$. A linear fit to the data for each of the values of $\overline{S^2}$ plotted is also included. These plots are essentially vertical cuts through the data of Fig. 1. The form of the linear fits in Fig. 4 is

$$K = \alpha + \beta(1/k). \tag{11}$$

The y-intercepts and slope of the linear fit to the K versus $1/k$ data, α and β respectively, are functions of $\overline{S^2}$, having the form,

$$\alpha = A_1\overline{S^2}, \tag{12}$$

$$\beta = A_2\overline{S^2}, \tag{13}$$

where A_1 and A_2 are the slopes of the fit to the

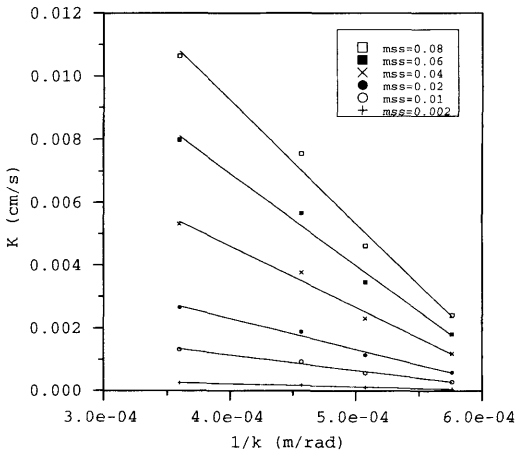

Fig. 4. Plot of K versus $1/k$ at several different values of $\overline{S^2}$. Lines faired through the data are linear fits.

$(\alpha, \overline{S^2})$ and $(\beta, \overline{S^2})$ data, respectively. Their values are $A_1 = 0.3102$ and $A_2 = -487.125$. In Fig. 5, α and β are plotted against $\overline{S^2}$. Combining eqs. (11) through (13) gives

$$K = A_1\overline{S^2} + A_2\overline{S^2}(1/k), \tag{14}$$

which permits computation of K for a given value of $\overline{S^2}$, and k.

Having developed a relationship for K as a function of k and $\overline{S^2}$, it now remains to define an algorithm for computing K_c, which is the value of

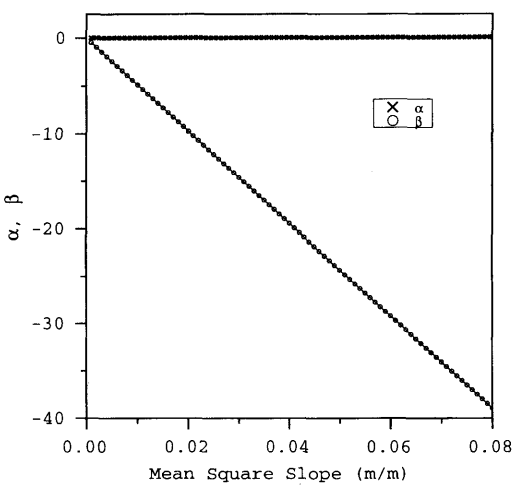

Fig. 5. Plot of α and β versus $\overline{S^2}$ for the range of $\overline{S^2}$ presented in Fig. 1. The solid lines are obtained from eqs. (12) and (13).

K due to all wave numbers in the range $k_1 < k < k_2$. First, the equation for $\overline{S^2}$, eq. (7), is rewritten using eq. (8) to give

$$\overline{S^2} = \int_{k_a}^{k_b} \phi(k)k^3 \, dk. \tag{15}$$

Next, defining the wave slope spectrum, $P(k)$

$$P(k) = \phi(k)k^3, \tag{16}$$

$\overline{S^2}$ is again rewritten as

$$\overline{S^2} = \int_{k_a}^{k_b} P(k) \, dk. \tag{17}$$

For a sufficiently small wave number interval, $\Delta k = k_b - k_a$, $P(k)$ can be accurately approximated as a linear function of k, and $\overline{S^2}$ can be approximated as

$$\overline{S^2} = P(k_i)\Delta k, \tag{18}$$

where

$$k_i = \frac{(k_a + k_b)}{2}. \tag{19}$$

Below this small value of Δk, it follows from eq. (18) that changing Δk by a constant factor will change $\overline{S^2}$ by that same factor. Similarly, from eq. (2), it is also true that changing $\overline{S^2}$ by a constant factor changes K by that same factor. The net result is that below a critical value of Δk, the value of K in the interval $k_a < k < k_b$ is linearly related to the size of that interval. Hence, K_c can be computed by simply summing the value of K in each interval Δk, over the entire range in k, $k_1 < k < k_2$. That is,

$$K_c = \sum_{i=1}^{n} K_i, \tag{20}$$

where, K_i is obtained by inserting eq. (18) into eq. (14) to give

$$K_i = A_1 P(k_i)\Delta k + A_2 P(k_i)(1/k_i)\Delta k, \tag{21}$$

where

$$\Delta k = \frac{k_2 - k_1}{n - 1}. \tag{22}$$

The constancy of the summation in eq. (20) was checked by computing K_c using progressively smaller values of Δk. K_c was found to give results which were within 1% of the asymptotic value, when $\Delta k < 10$ rads/m.

2.2. K_{tot} *model*

The second part of the model for K_f is K_{tot} which is the total gas exchange coefficient attained at a given wind speed. Here, K_{tot} is used in the usual way to parameterize all processes which contribute to gas exchange (e.g., wave breaking, bubble entrainment, turbulence etc.) against wind speed. Such gas exchange coefficients are typically obtained from wind/wave tunnel experiments.

Two models for K_{tot} will be considered here. The first is a curve fit to the data of Ocampo-Torres et al. (1994), where the transport of CO_2 was measured as a function of the wind speed in a wind/wave tunnel. A 4th order polynomial was used to fit the data,

$$K_{tot} = a_1 u^4 + a_2 u^3 + a_3 u^2 + a_4 u + a_5, \qquad (23)$$

where $a_1 = 3.98 \times 10^{-8}$, $a_2 = -2.95 \times 10^{-6}$, $a_3 = 7.94 \times 10^{-5}$, $a_4 = -6.23 \times 10^{-5}$, $a_5 = 5.48 \times 10^{-4}$, u is in m/s at a height of 10 m and K_{tot} is in cm/s. A plot of this data, along with eq. (23) is presented in Fig. 6. It should be noted that the original wind speed data presented in Ocampo-Torres et al. (1994) was measured at a height of 0.3 m. This data was converted to the standard velocity at a height of 10 m, assuming a logarithmic velocity profile,

$$\frac{u - u_0}{u_*} = \frac{1}{\kappa} \ln\left(\frac{z}{z_0}\right), \qquad (24)$$

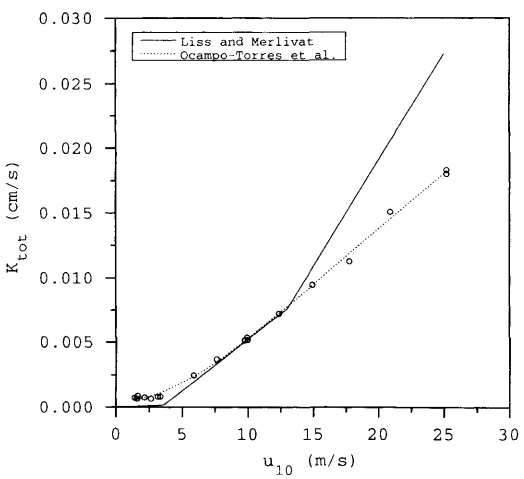

Fig. 6. K_{tot} versus wind speed models due to Liss and Merlivat (1986) and Ocampo-Torres et al. (1994). The models are described by eqs. (25) and (23), respectively.

where u_* is the friction velocity, u_0 is the speed of the water surface (0.1 m/s), κ is von Karman's constant, which was taken to be 0.4 (following Large and Pond, 1981), z_0 is the aerodynamic roughness, z, is height, and u is the wind speed at height z. Values for u_* were obtained from the Ocampo-Torres et al. (1994) data set.

The second model for K_{tot} used here is the Liss and Merlivat (1986) model, which is a piecewise linear model, consisting of three segments,

$$\begin{aligned} K_{tot} &= 4.72 \times 10^{-5} u & 0 \leqslant u \leqslant 3.6 \\ K_{tot} &= 7.92 \times 10^{-4} u - 2.68 \times 10^{-3} & 3.6 < u \leqslant 13 \\ K_{tot} &= 1.64 \times 10^{-3} u - 1.37 \times 10^{-2} & u > 13 \end{aligned} \qquad (25)$$

The Liss and Merlivat model for K_{tot} is also presented in Fig. 6. Note that u is the velocity at a height of 10 m in this relation as well.

Combining the two models for K_{tot} with the two models for K_c, four models for K_f are obtained. These 4 models are cataloged in Table 2 as models 1 through 4. The results obtained from these models are now described.

3. Results

Plots of K_f versus wind speed for each of the four models listed in Table 2 are presented in Fig. 7. Models 3 and 4 both give small values for K_f, except at very small wind speeds. This follows from the fact that the wave number spectra for the E-model gives values which are over an order of magnitude smaller than for the A-model, and these results propagate through to the K_f model. Model 2 displays discontinuities at the wind speeds $u = 3.6$ m/s and $u = 13$ m/s, giving K_f values of 8% and 4%, respectively. These discontinuities are located at the breaks in the piecewise linear

Table 2. *Catalogue of the 4 models, constructed using the indicated model for wave number spectrum, and* K_{tot}

Model #	Ψ model	K_{tot} model
1	A-model	Ocampo-Torres et al. (1994)
2	A-model	Liss and Merlivat (1986)
3	E-model	Ocampo-Torres et al. (1994)
4	E-model	Liss and Merlivat (1986)

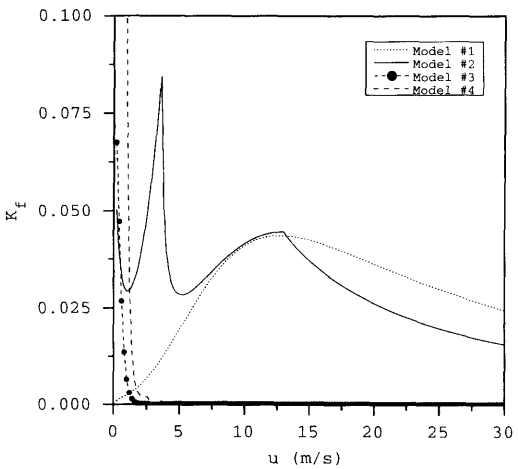

Fig. 7. K_f versus wind speed for the four different combinations of K_{tot} and K_c models. The models are tabulated in Table 2.

plot of the Liss and Merlivat (1986) K_{tot} relation (eq. (25)). The K_f values located at these discontinuities, particularly the large spike located at $u = 3.6$ m/s, are probably more a reflection of the inaccuracy of this K_{tot} relationship than an indication of particularly high values for K_f at these two wind speeds. Model 1 displays a continuous, smooth K_f versus u relationship with a peak of 4% at 12.8 m/s.

Since the models for K_f require only u as an input, remotely sensed wind speed data can be used as the model input, providing global maps of K_f. Global wind speed data was obtained from passive microwave radiometric measurements from the Defense Meteorological Satellite Program (DMSP) Special Sensor Microwave Imager (SSM/I). These measurements are provided in the form of wind speed by the NOAA National Climatic Data Center (NCDC). The SSM/I is a four frequency, linearly-polarized, passive microwave radiometric system. Measurements are obtained at 19.35, 22.24, 37.0 and 85.5 GHz. The passive radiometric data is converted to wind speed, by NOAA, at $1° \times 1°$ resolution, using the algorithm of Goodberlet et al. (1989) and using a weather screen due to Ferraro et al. (1994) for rain detection. These wind speeds are referenced at a height of 19.5 m and were converted to the standard 10 m height, as described in Section 2.

The data provided by NCDC is in the form of wind speed maps, where each pixel consists of a monthly averaged wind speed, and spans the years 1988 to present. Presenting this data in the form of maps over this span of time is impractical. Instead, plots of the global average are presented as a function of month for 118 months. The wind speed is used as an input to the K_f models developed above. In Fig. 8a, K_f is plotted against month for models 1 and 2. These two models give values which fall between 3–4% for all months investigated. The K_f results for models 3 and 4 are presented in Fig. 8b, yielding extremely small

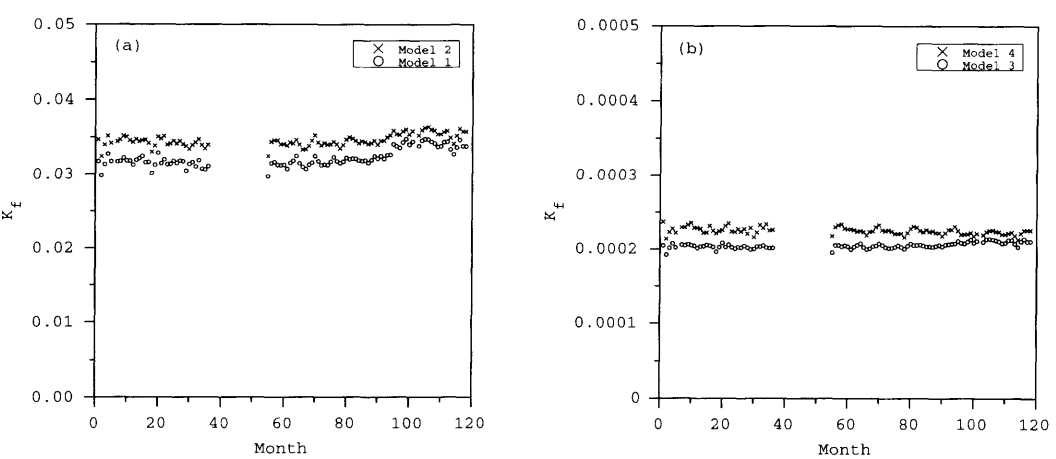

Fig. 8. Plot of K_f, averaged over the entire ocean surface for each month. Month 1 corresponds to July 1987 and the last month corresponds to April, 1997. (a) Models 1 and 2, (b) Models 3 and 4 (Table 2).

values, less than 0.03% for all months. The blank region located roughly in the center of each plot corresponds to a period of instrument failure.

As mentioned earlier, K_f was computed only for the range of wave numbers described by eqs. (5) and (6) since the only monochromatic data for K which exists lies in this range. As an exercise, the models for K_f were recomputed for all capillary waves, that is all wave numbers greater than $k =$ 370 rads/m, by extrapolating the experimental data of Saylor and Handler (1997). Plots of K_f versus u are presented for this wave number range in Fig. 9. These plots display values which, while larger for all cases, do not differ significantly from the results displayed in Fig. 7. This is an interesting point, since it seems to suggest that wave numbers outside of the range used to compute the plots in Fig. 7 do not contribute significantly to K_f. This in turn suggests that the capillary waves which contribute most significantly to K_f may lie in, or near, the range explored. To test this hypothesis, the product of K (eq. (14)) and ϕ (eq. (8)) was plotted for a range of $\overline{S^2}$ in Fig. 10a and a range of u in Fig. 10b. In both figures, the A-model was used for ϕ. The peak in both figures is located at $k = 1790$ rads/m ($\lambda = 3.5$ mm) and is independent of $\overline{S^2}$ and u. This process was repeated for the E-model, yielding a peak at $k = 1690$ rads/m ($\lambda =$ 3.7 mm), which was also independent of $\overline{S^2}$ and u. The small difference between these two values is remarkable in light of the enormous variation between the magnitudes and form of the two wave number spectra. These results suggest that, of all capillary waves, those having wavelengths around 3.6 mm contribute most to gas exchange.

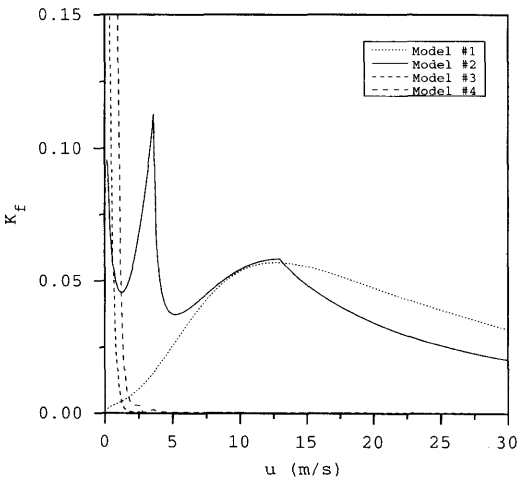

Fig. 9. K_f versus wind speed extrapolated for all capillary wave numbers. The models are tabulated in Table 2.

4. Discussion

The four models for K_f plotted in Fig. 7 show significant differences in behavior and magnitude and these are now discussed. Of the four models,

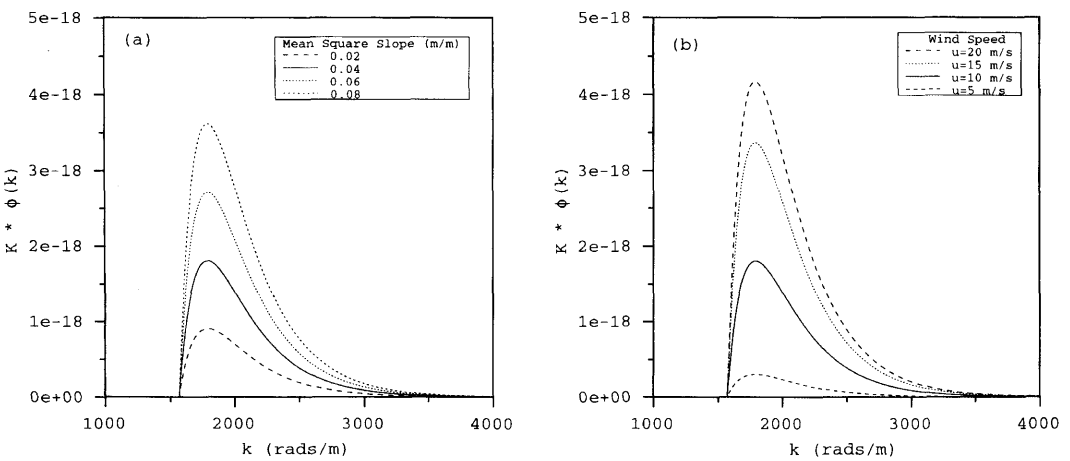

Fig. 10. The product of K and ϕ. (a) Wind speed 10 m/s for several different values of $\overline{S^2}$. (b) $\overline{S^2} = 0.04$ m/m and wind speed is varied.

model 2 exhibits the most anomalous behavior, displaying two discontinuities in the K_f versus u plot. As stated in the previous section, these discontinuities are due to the discontinuity in the Liss and Merlivat (1986) model for K_{tot}. Hence, the sharp peaks displayed in Fig. 7 are almost certainly non-physical, and hence this model, as well as model 4, which also uses this K_{tot} relationship will not be considered further.

This leaves models 1 and 3, which both use the Ocampo-Torres et al. (1994) model for K_{tot}. Model 3 exhibits small values for K_f, except at very low wind speeds, where it peaks at $\sim 7\%$. Model 1 exhibits small values for K_f when the wind speed is small, and peaks at a wind speed of about $u = 13$ m/s, where $K_f = 4\%$. The reason for this difference in behavior is due to the different models used for the wave height spectrum. As illustrated in Figs. 2b and 3b, at all wind speeds above about 2 m/s, the A-spectrum gives values which exceed the E-spectrum by at least two orders of magnitude at all wave numbers in the range $k_1 < k < k_2$. However, while the A-spectrum continues to decrease with decreasing wind speed, once u drops below 1 m/s, the E-spectrum actually increases, exhibiting values which exceed the A-model at all wave numbers in the range $k_1 < k < k_2$. This accounts for the large K_f values at low wind speed, for model 3. These large values at small u minimally affect the globally averaged values for K_f. The globally averaged wind speed is approximately 8 m/s and the large values of K_f below $u = 1$ m/s do not significantly contribute to this averaged K_f.

Models 1 and 3 differ only in the choice of wave height spectrum. For the high wave numbers considered here, there has been no experimental validation of $\phi(k)$, and it is impossible, therefore, to determine which of the existing wave height spectra, if any, are accurate. As a result, it is not yet possible to make a strong statement concerning the numerical accuracy of the K_f models presented herein. It is possible that the values of K_f reported here may actually be underpredictions, should the models of $\phi(k)$ used turn out to be too small in the wave number range $k_1 < k < k_2$. There is, in fact, evidence which suggests that this may be the case. Hwang et al. (1996) have obtained wave spectra in the ocean, resolved to a minimum wavelength of 4 mm, and have found that the spectra are significantly larger than complementary data obtained in wind/wave tunnels in the range $k = 100$–1000 rad/m. The reason for this difference was postulated to be the presence of variations in wind speed and wind direction which exist in the ocean, but are completely absent in laboratory measurements. This is an important point, since the E- and A-models employed in the present work utilize laboratory data to construct the wave spectrum. While the data of Hwang et al. (1996) does not extend to the wave numbers investigated in this work, it is likely that $\phi(k)$ is indeed larger than predicted by either the E- or A-spectra, at these high wave numbers, and consequently that K_f is also larger. While these conclusions are somewhat tentative, they do demonstrate the importance of extending existing measurements of $\phi(k)$ to higher wave numbers.

The K_f values plotted in Figs. 8a,b were obtained using a monthly averaged wind speed as the model input. Because of the nonlinear K_f versus u behavior for all of the models, it is possible that the globally averaged values of K_f would be different had a more frequently sampled wind speed been used as the model input. For example, in the case of model 3 an average wind speed of 4 m/s would yield a negligible value for K_f. However, if that averaged wind speed arose from winds which varied from 1 m/s during one portion of the averaging cycle, to 7 m/s during the other part of the cycle, the average wind speed would be 4 m/s, yet the values of K_f during the 1 m/s winds would be significant, resulting in an averaged K_f, much larger than that obtained from the average wind speed.

A different, but related, point concerns transient winds, or wind gusts. Studies on the temporal evolution of the wave slope spectrum have demonstrated that the high wave number portion of the spectrum develops first and that the lower wave numbers mature much later. Furthermore, the work of Wu (1979) shows that not only does the high wave number portion of the spectrum grow faster during growing winds, but the frequency of occurrence of high wave number slopes during early times is even greater than during steady times. This indicates that the numerical value of the spectrum at high wave numbers may be larger during wind gusts than during steady state, even at an equivalent wind speed. This points toward a larger than expected rôle of capillary waves in regions where wind gusts are prevalent. However,

it is not possible to state whether K_f would actually be larger in such regions, since the behavior of K_{tot} is unknown during wind gusts (to the best of the author's knowledge). Hwang et al. (1996) have noted that variations in wind speed and wind direction may be responsible for the larger values observed in the high wave number portion of their spectrum, compared to laboratory data. Laboratory data is obtained at a constant wind speed and direction, which permits the development of a spectral gap at the wave number corresponding to the minimum phase speed. In the ocean, variations in wind speed and direction prevent the formation of such a gap, and may account for the larger values of $\phi(k)$ observed by Hwang et al. (1996). These results indicate that experimentally obtained spectra in wind/wave tunnels may underpredict $\phi(k)$ at high wave numbers.

The model for K_c used here employs data obtained from Faraday waves. As discussed in Section 1, these waves are standing waves at very low excitation amplitudes, but for the experiments of Saylor and Handler (1997), this standing wave pattern continuously drifted about. While the presence of this drift avoided the problem of having enhanced transport only at fixed locations on the water surface, it is nevertheless possible that the underlying hydrodynamics of these drifting Faraday waves may be so different from progressive waves as to result in significantly different gas exchange. Existing studies of Faraday waves seem to indicate that this is not the case. Gollub and co-workers have demonstrated that drifting Faraday waves can be understood as a random fluctuation of the Stokes drift (Ramshankar et al., 1990; Mesquita et al., 1992), similar to that which occurs on a random field of ocean waves. Using a model developed by Herterich and Hasselmann (1982), for horizontal dispersion of tracers in a random field of ocean surface waves, they demonstrate that Faraday waves which exhibit a random drift effect a horizontal dispersion which agrees with the oceanic model of Herterich and Hasselmann to within a factor of 3 for excitation amplitudes comparable to the work of Saylor and Handler (1997). While this result is for horizontal transport, it seems reasonable to expect similar agreement for vertical transport.

Evidence also exists in the sediment transport literature, for a similarity between the transport which occurs for standing and progressive gravity waves. For example, Iskandarani and Liu (1991) demonstrate that the vertical mass transport velocities are comparable for three dimensional progressive and standing gravity waves. Similarly, Hsu et al. (1980) show that short-crested waves created by combining two progressive waves at an angle of 45°, result in vertical mass transport which differs by at most a factor of 3 from the standing wave case. While these studies are for shallow gravity waves, and not for the capillary waves considered here, the results seem to indicate that even if the Faraday waves had been of the non-drifting, standing wave type, the values of K_f obtained here should not differ significantly if they had been obtained from pure progressive capillary waves.

In the process of developing the models for K_f described in this paper, an interesting ancillary result was uncovered. The data plotted in Fig. 4 shows that, for a constant $\overline{S^2}$, K is a linear function of inverse wave number. For linear capillary waves, the total energy density E is described as (Phillips, 1966),

$$E = \rho\sigma\overline{S^2}, \tag{26}$$

where ρ is the water density and σ is the surface tension. Eq. (26) shows that the total energy (potential and kinetic) contained in the wave field is independent of wave number at constant mean square slope. Each line in Fig. 4 is, therefore, a constant energy line. Hence, for the range of capillary waves investigated, the gas exchange coefficient of capillary waves increases as the wavelength gets smaller without any extra input of energy into the system. This result is most likely a reflection of the fact that the concentration boundary layer beneath the waves is much thinner than the wavelengths investigated, and hence reducing λ brings the scale of the wave closer to that of the boundary layer, allowing the wave energy to couple more directly with the gas exchange process.

Finally, it is noted that wave slope spectra display a decrease in the spectral value as the wave number increases, while K displays an increase with increasing wave number. This behavior suggests a peak in the product of K and ϕ which was indeed observed (Fig. 10). The location of this peak is at a wavelength of 3.5 mm when the A-model is used for ϕ, and a wavelength of 3.7 mm when the E-model is used for ϕ. These

results suggest that small capillary waves play an important rôle in gas exchange, but that it is a very specific band of capillary waves, having wavelengths around 3.6 mm which contribute most to gas exchange. This result is obtained by extrapolating the data of Saylor and Handler (1997) outside the range they investigated, and relies on the implicit assumption that the linear behavior of the K versus $1/k$ data displayed in Fig. 4 will exist outside of the range $k_1 < k < k_2$. While this assumption may not strictly hold, it seems unlikely that a dramatic change in the K versus $1/k$ behavior will occur outside of this range. Nevertheless, the conclusion concerning the location of the peak contribution of capillary wave gas exchange at $\lambda = 3.6$ mm, must be viewed as somewhat tentative, and further experiments in this area would be useful. It should be noted that while uncertainties are introduced in the process of extrapolating the data of Saylor and Handler (1997), the orders of magnitude difference between wave spectra models which exists is the largest source of uncertainty in the K_f model presented here. It seems, therefore, that a better prediction of K_f will result from more accurate and realistic measurements of $\phi(k)$.

5. Conclusion

A model was developed to estimate K_f, the contribution of capillary waves to the oceanic gas exchange coefficient. Although capillary waves were shown to significantly enhance gas exchange in the laboratory, the small wave energies predicted by existing wave height spectra resulted in relatively small values for K_f. Global averages of K_f were estimated to be less than 4%. It was noted that the high wave number portion of the wave height spectrum has not been experimentally validated, and that such experiments are necessary to predict K_f with greater confidence. This is an especially noteworthy point in light of the orders of magnitude variation between wave height spectra models which currently exists. It was also noted that spectra obtained in the ocean display much larger values than laboratory spectra in the capillary wave regime. These differences are presumed to be due to variations in wind speed and wind direction which exist on the ocean, but not in the laboratory. Since models for ϕ rely on laboratory data, there is a high probability that ϕ is larger in the ocean, and therefore K_f is larger than predicted here. It was shown that a peak in the contribution of capillary waves to the gas exchange coefficient occurs around $\lambda = 3.6$ mm, and is independent of wind speed and $\overline{S^2}$. Finally, it was demonstrated that, for capillary waves, K increases linearly with inverse wave number at constant $\overline{S^2}$. Since the total wave energy density is linearly related to $\overline{S^2}$, a concomitant result it that, for the range of wave numbers investigated here, large increases in gas exchange occur at constant energy input when the wavelength is decreased.

6. Acknowledgements

The encouragement and insightful comments of Robert A. Handler are gratefully acknowledged. The author would like to thank Arnie Cooper, George Marmorino, Geoffrey B. Smith, Richard I. Leighton and Walter McKeown for useful comments and discussions. Satellite data was obtained from the NOAA National Geophysical Data Center. The technical assistance of Ralph Ferraro (NOAA/NESDIS/ORA) is also acknowledged. Financial support was provided by the Office of Naval Research through the Naval Research Laboratory, and the National Research Council. Computational support was provided by the High Performance Computer Modernization Program (HPCMP).

REFERENCES

Allen, K. R. and Joseph, R. I. 1990. A canonical statistical theory of surface wind waves. EOS. *Trans. Am. Geophys. U.* **71**, 73.

Apel, J. R. 1994. An improved model of the ocean surface wave vector spectrum and its effects on radar backscatter. *J. Geophys. Res.* **99**, 16279–16291.

Banner, M. L. 1990. Equilibrium spectra of wind waves. *J. Phys. Oceanog.* **20**, 966–984.

Benjamin, T. B. and Ursell, F. 1954. The stability of the plane free surface of a liquid in vertical periodic motion. *Proc. R. Soc. London, Ser. A* **225**, 505–515.

Bjerkaas, A. W. and Riedel, F. W. 1979. *Proposed model*

for the elevation spectrum of a wind-roughened sea surface. TG 1382, The Johns Hopkins University, Applied Physics Laboratory.

Broecker, H.-C., Petermann, J. and Siems, W. 1978. The influence of wind on CO_2 exchange in a wind-wave tunnel, including the effects of monolayers. *J. Mar. Res.* **36**, 595–610.

Christiansen, B., Alstrom, P. and Levinsen, M. T. 1995. Dissipation and ordering in capillary waves at high aspect ratios. *J. Fluid Mech.* **291**, 323–341.

Donelan, M. A. and Pierson, W. J. 1987. Radar scattering and equilibrium ranges in wind-generated waves with application to scatterometry. *J. Geophys. Res.* **92**, 4971–5029.

Elfouhaily, T., Chapron, B., Katsaros, K. and Vandemark, D. 1997. A unified directional spectrum for long and short wind-driven waves. *J. Geophys. Res.* **102**, 15781–15796.

Faraday, M. 1831. On the forms and states assumed by fluids in contact with vibrating elastic surfaces. *Philos. Trans. R. Soc. London* **121**, 319–340.

Ferraro, R. R., Grody, N. C. and Marks, G. F. 1994. Effects of surface conditions on rain identification using the SSM/I. *Remote Sens. Rev.* **11**, 195–209.

Goodberlet, M. A., Swift, C. T. and Wilkerson, J. C. 1989. Remote sensing of ocean surface winds with the special sensor microwave imager. *J. Geophys. Res.* **94**, 14544–14555.

Henderson, D. M. and Miles, J. W. 1990. Single-mode Faraday waves in small cylinders. *J. Fluid Mech.* **213**, 95–109.

Henderson, D. M. and Miles, J. W. 1991. Faraday waves in 2 : 1 internal resonance. *J. Fluid Mech.* **222**, 449–470.

Herterich, K. and Hasselmann, K. 1982. The horizontal diffusion of tracers by surface waves. *J. Phys. Oceanog.* **12**, 704–711.

Hsu, J. R. C., Silvester, R., and Tsuchiya, Y. 1980. Boundary-layer velocities and mass transport in short-crested waves. *J. Fluid Mech.* **99**, 321–342.

Hwang, P. A., Atakturk, S., Sletten, M. A. and Trizna, D. B. 1996. A study of the wavenumber spectra of short water waves in the ocean. *J. Phys. Oceanog.* **26**, 1266–1285.

Iskandarani, M. and Liu, P. L.-F. 1991. Mass transport in three-dimensional water waves. *J. Fluid Mech.* **231**, 417–437.

Jähne, B., Münnich, K. O. and Siegenthaler, U. 1979. Measurements of gas exchange and momentum transfer in a circular wind-water tunnel. *Tellus* **31**, 321–329.

Jähne, B., Wais, T., Memery, L., Caulliex, G., Merlivat, L., Münnich, K. O. and Coantic, M. 1985. He and Rn gas exchange experiments in the large wind–wave facility of IMST. *J. Geophys. Res.* **90**, 11989–11997.

Jähne, B., Münnich, K. O., Bösinger, R., Dutzi, A., Huber, W. and Libner, P. 1987. On the parameters influencing air–water gas exchange. *J. Geophys. Res.* **92**, 1937–1949.

Jähne, B. and Riemer K. S. 1990. Two-dimensional wave number spectra of small-scale water surface waves. *J. Geophys. Res.* **95**, 11531–11546.

Kitaigorodskii, S. A. 1983. On the theory of the equilibrium range in the spectrum of wind generated gravity waves. *J. Phys. Oceanog.* **13**, 816–827.

Klinke, J. and Jähne, B. 1992. 2D wave number spectra of short wind waves: results from wind wave facilities and extrapolation to the ocean. In: *Optics of the air-sea interface; theory and measurements* (ed. L. Estep). SPIE Proc. 1749, 1–13.

Large, W. G. and Pond, S. 1981. Open ocean momentum flux measurements in moderate to strong winds. *J. Phys. Oceanog.* **11**, 324–336.

Liss, P. and Merlivat, L. 1986. Air-sea gas exchange rates: Introduction and synthesis. In: *The rôle of air–sea gas exchange in geochemical cycling* (ed. P. Buat-Ménard). Adv. Sci. Inst. Ser. D. Reidel Pub. Co., 113–127.

Mesquita, O. N., Kane, S. and Gollub, J. P. 1992. Transport by capillary waves: Fluctuating Stokes drift. *Phys. Rev.* **A45**, 3700–3705.

Miles, J. W. and Henderson, D. M. 1990. Parametrically forced surface waves. *Ann. Rev. Fluid Mech.* **22**, 143–165.

Miles, J. W. 1993. On Faraday waves. *J. Fluid Mech.* **248**, 671–683.

Milner, S. T. 1991. Square patterns and secondary instabilities in driven capillary waves. *J. Fluid Mech.* **225**, 81–100.

Ocampo-Torres, F. J., Donelan, M. A., Merzi, N. and Jia, F. 1994. Laboratory measurements of mass transfer of carbon dioxide and water vapour for smooth and rough flow conditions. *Tellus* **46B**, 16–32.

Phillips, O. M. 1958. The equilibrium range in the spectrum of wind-generated waves. *J. Fluid Mech.* **4**, 426–434.

Phillips, O. M. 1966. *The dynamics of the upper ocean,* London: Cambridge University Press.

Pierson, W. J. and Moskowitz, L. 1964. A proposed spectral form for fully developed wind seas based on the similarity theory of S. A. Kitaigorodskii. *J. Geophys. Res.* **69**, 5181–5190.

Ramshankar, R., Berlin, D., and Gollub, J. P. 1990. Transport by capillary waves. Part I. Particle trajectories. *Phys. Fluids* **2**, 1955–1965.

Saylor, J. R. and Handler, R. A. 1997. Gas transport across an air/water interface populated with capillary waves. *Phys. Fluids* **9**, 2529–2541.

Szeri, A. J. 1997. Capillary waves and air-sea gas transfer. *J. Fluid Mech.* **332**, 341–358.

Vanden-Broeck, J.-M. 1984. Nonlinear gravity-capillary standing waves in water of arbitrary uniform depth. *J. Fluid Mech.* **139**, 97–104.

Wu, J. 1972. Sea-surface slope and equilibrium wind-wave spectra. *Phys. Fluids* **15**, 741–747.

Wu, J. 1979. Temporal rates of growth and decay of microscopic and macroscopic surface structures in a wind-wave tank. *J. Phys. Oceanog.* **9**, 802–814.